Indian J Phys (September 2015) 89(9):923–929
DOI 10.1007/s12648-015-0671-2

ORIGINAL PAPER

Non-centrosymmetric $LiBaB_9O_{15}$ single crystal: growth and characterization

A H Reshak[1,2]*, X Chen[3], H Kamarudin[2], Y Chen[3] and S Auluck[4]

[1]New Technologies - Research Center, University of West Bohemia, Univerzitni 8, 306 14 Pilsen, Czech Republic

[2]Center of Excellence Geopolymer and Green Technology, School of Material Engineering, University Malaysia Perlis, 01007 Kangar, Perlis, Malaysia

[3]College of Materials Science and Engineering, Beijing University of Technology, Ping Le Yuan 100, Beijing 100124, People's Republic of China

[4]National Physical Laboratory, Dr. K S Krishnan Marg, New Delhi 110012, India

Received: 04 November 2014 / Accepted: 05 February 2015 / Published online: 13 March 2015

Abstract: The non-centrosymmetric $LiBaB_9O_{15}$ single crystal was synthesized by employing high-temperature solution reaction methods at 830 °C. Single-crystal X-ray diffraction analysis showed that it crystallized in the non-centrosymmetric space group *R3c*, with cell dimensions $a = 10.973(1)$ Å, $c = 17.049(2)$ Å, $Z = 6$ and $V = 1777.8(3)$ Å^3, having 3D frameworks consisting of $[B_3O_7]^{5-}$ groups bridged by O atoms, with channels occupied by Li^+ and Ba^{2+} cations. The atomic positions taken from X-ray diffraction data were optimized by minimizing the forces acting on the atoms. From the relaxed geometry, the electronic structure and the chemical bonding were determined and various spectroscopic features were calculated and compared with experimental data. The state-of-the-art all-electron full-potential linearized augmented plane wave method within the Ceperley–Alder local density approximation and the gradient approximation was used to solve the Kohn–Sham density functional theory equations. Very good agreement between the measurements and the calculations was found. The calculated effective mass ratio of heavy holes (m^*_{hh}/m_e), light holes (m^*_{lh}/m_e) and electrons (m^*_e/m_e) was 0.4670, 0.0973 and 0.0120, respectively.

Keywords: Electronic materials; Inorganic compounds; Optical materials; Crystal growth; X-ray diffraction; Crystal structure; Optical properties

PACS Nos.: 71.15.-m; 71.20.Nr

1. Introduction

In last few decades, a lot of research has been carried out on borate materials [1–10]. In the ternary Li_2O–BaO–B_2O_3 system, three ternary phases, $LiBaBO_3$, $LiBa_2B_5O_{10}$ and $LiBaB_9O_{15}$, have been previously found and their crystal structures have been determined from single-crystal X-ray diffraction (XRD) data [11–14]. The ternary compound $LiBaB_9O_{15}$ exists in two different phases. The first phase (space group *R 3 c*) has been synthesized using the solid-state reaction method [13], whereas the second phase [space group (*R −3 c*)] has been synthesized using hydrothermal method [14]. These structures (*R 3 c* and *R −3 c*) are reported to have three-dimensional networks built from triborate $[B_3O_7]^{5-}$ groups.

While attempting to prepare these new non-centrosymmetric compounds that are potentially applicable as nonlinear optical (NLO) materials, we have obtained single crystals of $LiBaB_9O_{15}$. Our single-crystal X-ray diffraction data show that $LiBaB_9O_{15}$ single crystals possess the *R 3 c* space group in excellent agreement with that obtained by Penin et al. [13]. The $LiBaB_9O_{15}$ single crystal crystallizes in the non-centrosymmetric space group, which results in interesting NLO properties [15], photoinduced NLO absorption, elasto-optics, fluorescence matrix elements and

Electronic supplementary material The online version of this article (doi:10.1007/s12648-015-0671-2) contains supplementary material, which is available to authorized users.

*Corresponding author, E-mail: maalidph@yahoo.co.uk

piezoelectricity [16–19]. We would like to mention that the crystals possess high laser stability.

The IR spectrum further confirms the presence of both BO_3 and BO_4 groups [15]. UV–visible diffuse reflectance spectrum shows a band gap of about 5.17 eV [15]. Solid-state fluorescence spectrum exhibits the emission main peak at around 515 nm and a shoulder at 430 nm [15]. Although its crystal structure has been previously determined, no IR, UV–visible diffuse reflectance and emission spectra as well as first principle calculations on the electronic band structure, density of states, the electronic charge density distribution and the chemical bonding properties for $LiBaB_9O_{15}$ are available in the literature. In this work, we report results of the experimental measurements mentioned above and theoretical calculations so as to make a meaningful comparison.

2. Experimental details

Single crystals of $LiBaB_9O_{15}$ were grown from the high-temperature solution using $BaCO_3$, ZnO, H_3BO_3 and Li_2CO_3 (molar ratio = 4:4:26:3) as the starting materials at a reaction temperature of 830°. A small crystal with dimensions of $0.20 \times 0.10 \times 0.10$ mm^3 was carefully selected under an optical microscope and X-ray intensity data were collected on an automated Rigaku AFC7R four-circle diffractometer using monochromatized Mo Kα radiation. The data reduction was performed using RIGAKU/AFC Diffractometer Control Software [20] with the intensities corrected for Lorentz and polarization effects and for absorption by empirical method based on ψ-scan data. The crystal structure was solved by direct methods [21] and refined in SHELX-97 system [22] by full-matrix least-squares methods on F_o^2. All of the atoms were refined with positional as well as anisotropic displacement parameters. Due to the low data to parameters ratio, restraints were added to improve the refinement. Details of crystal parameters, data collection and structure refinements are given in Table 1. The atomic coordinates and the equivalent isotropic displacement parameters are shown in Tables 2 and 3 and the selected bond lengths and angles are listed in Tables 4 and 5, respectively. For more details about $LiBaB_9O_{15}$ single crystal. The crystallographic Information Framework (CIF) was depicted as supplementary material, available in online version.

Table 1 Crystallographic data for $LiBaB_9O_{15}$

Formula	$LiBaB_9O_{15}$
T (K)	290
λ (Å)	0.71073
Crystal system	Trigonal
Space group	*R 3 c* (No. 161)
a (Å)	10.973(1)
c (Å)	17.049(2)
V (Å^3), Z	1777.8(3), 6
d_{calc} (g/cm^3)	2.699
μ (mm^{-1})	3.442
$2\theta_{max}$ (°)	54.96
Reflections collected	901
Unique reflection	470
Observed [$I \geq 2\sigma(I)$]	431
R_{int}	0.0212
Number of variables	79
Number of restraints	79
Flack parameter	0.00(8)
GOF on F_o^2	1.101
R1/wR2 [$I \geq 2\sigma(I)$]	0.0174/0.0475
R1/wR2 (all data)	0.0194/0.0485
Largest difference map peak and hole (e Å^{-3})	0.387 and −0.669

Table 2 Atomic coordinates and equivalent isotropic displacement parameters (Å^2) for $LiBaB_9O_{15}$

Atoms	*X*	*Y*	*Z*	U_{eq}
Li1	0	0	0.2330(12)	0.025(7)
Ba1	0	0	−0.0010(2)	0.01305(13)
B1	0.3993(10)	0.2703(10)	0.0241(5)	0.0093(5)
B2	0.4650(9)	0.3998(10)	0.1470(5)	0.0095(5)
B3	0.2361(7)	0.3330(13)	0.0855(7)	0.0093(5)
O1	0.4978(4)	0.3389(7)	0.0813(5)	0.0118(4)
O2	0.2688(7)	0.2505(6)	0.0303(3)	0.0117(4)
O3	0.2192(8)	0.4381(13)	0.0381(4)	0.0116(4)
O4	0.3473(6)	0.4116(6)	0.1418(3)	0.0112(4)
O5	0.1086(7)	0.2247(13)	0.1246(4)	0.0110(4)

U_{eq} is defined as one-third of the trace of the orthogonalized U tensor

3. Theoretical calculation

The atomic positions of $LiBaB_9O_{15}$ single crystal taken from our X-ray diffraction data shown in Table 2 were optimized by minimization of the forces (1 mRy/au) acting on the atoms. The optimized atomic coordinates shown in Table 3 were in good agreement with the measured ones. From the relaxed geometry, the electronic structure and the chemical bonding were determined and various spectroscopic features were simulated and compared with experimental data. Once the forces were minimized in this construction, one could then find the self-consistent density at these positions by turning off the relaxations and driving the system to self-

Table 3 Optimized atomic coordinates for $LiBaB_9O_{15}$

Atoms	*X*	*Y*	*Z*
Li1	0.0	0.0	0.23290
Ba1	0.0	0.0	0.99878
B1	0.39778	0.26987	0.02410
B2	0.45988	0.24000	0.14324
B3	0.23645	0.32999	0.08110
O1	0.48992	0.33241	0.07998
O2	0.26211	0.25101	0.03100
O3	0.21395	0.43132	0.03798
O4	0.34101	0.40998	0.14089
O5	0.10911	0.22010	0.12399

Table 4 Selected bond lengths (Å) for $LiBaB_9O_{15}$

Bond lengths	Exp	Theory
Li1–O1 (×3)	1.902(4)	1.900
Li1–O5 (×3)	2.825(18)	2.811
Ba1–O2 (×3)	2.904(6)	2.899
Ba1–O4 (×3)	2.907(6)	2.899
Ba1–O5 (×3)	3.024(9)	3.011
Ba1–O3 (×3)	3.074(10)	2.991
B1–O2	1.341(11)	1.299
B1–O1	1.367(11)	1.378
B1–O5	1.405(11)	1.398
B2–O3	1.290(12)	1.289
B2–O4	1.364(10)	1.343
B2–O1	1.440(10)	1.421
B3–O4	1.449(13)	1.435
B3–O5	1.467(14)	1.442
B3–O2	1.470(12)	1.465
B3–O3	1.494(15)	1.500

Table 5 Selected bond angles (°) for $LiBaB_9O_{15}$

Bond angles	Exp	Theory
O2–B1–O1	121.3(7)	121.2
O2–B1–O5	121.6(9)	120.9
O1–B1–O5	117.1(8)	116.9
O3–B2–O4	124.0(9)	123.8
O3–B2–O1	118.4(9)	117.9
O4–B2–O1	117.5(7)	117.0
O4–B3–O5	111.1(9)	111.8
O4–B3–O2	113.5(8)	112.9
O5–B3–O2	102.7(9)	102.9
O4–B3–O3	106.9(9)	107.1
O5–B3–O3	115.8(8)	115.0
O2–B3–O3	106.9(8)	106.1

consistency. The state-of-the-art, all-electron full-potential linearized augmented plane wave (FP-LAPW) method was used to solve the Kohn–Sham DFT equations within the framework of the WIEN2k code [23]. This is an implementation of the DFT [24] with different possible approximation for the exchange correlation potentials. We used the Ceperley–Alder local density approximation (LDA) [25, 26] and Perdew–Becke–Ernzerhof gradient approximation (GGA) [27], which were based on exchange correlation energy optimization to calculate the total energy. The potential and charge density in the muffin-tin (MT) spheres were expanded in spherical harmonics with $l_{max} = 8$ and nonspherical components up to $l_{max} = 6$. The self-consistent calculations were converged since the total energy of the system was stable within 10^{-5} Ry. Self-consistency was obtained using 200 $\vec{k}$ points in the irreducible Brillouin zone (IBZ). The band structure, densities of states and the electron charge densities were calculated using 800 k points in the IBZ.

4. Results and discussion

As seen from Fig. 1 and Table 2, the asymmetric unit of $LiBaB_9O_{15}$ contains ten independent atoms, i.e., 1Li, 1Ba, 3B and 5O, of which Li and Ba atoms lie on crystallographic threefold axes and other atoms occupy general positions. Each Li^+ ion is strongly bonded to three O atoms at distances of 1.902(4) Å and also weakly bonded to three more O atoms at distances of 2.825(18) Å, as shown in

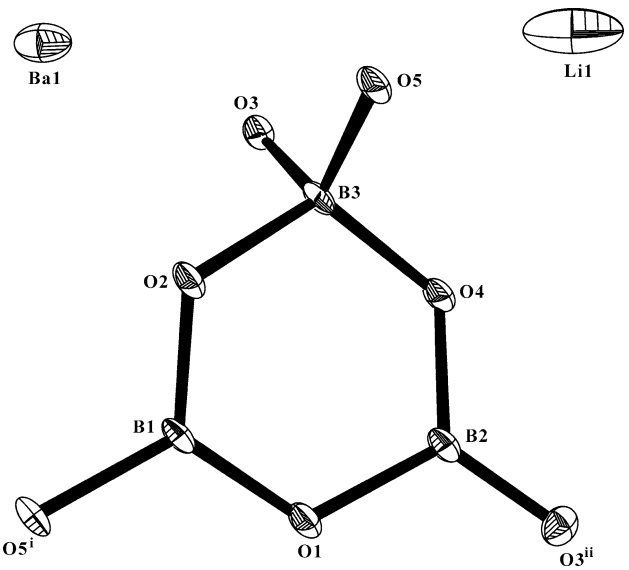

Fig. 1 Oak Ridge Thermal Ellipsoid Plot Program (ORTEP) view of the asymmetric unit of $LiBaB_9O_{15}$ to show the atomic labeling scheme. Displacement *ellipsoids* are drawn at 50 % probability level. Symmetry codes: i (0.6667 − y, 0.3333 − x, −0.1667 + z); ii (0.3333 + x, 0.6667 + x − y, 0.1667 + z)

Table 3. Taking all these six bonds into account, the concept of bond valence [28] allows us to calculate a bond valence sum (BVS) equal to 0.999 for Li1, which proves that the long bonds indeed participate in the metal coordination scheme. The sixfold coordination around Li can be described as a distorted trigonal antiprism. Each Ba^{2+} is coordinated to twelve O atoms arranged in a distorted cuboctahedral geometry with Ba–O distances of 2.904(6)–3.074(10) Å (average 2.977 Å, Table 3), which is comparable to the value 2.97 Å computed from crystal radii for a 12-coordinated Ba^{2+} ion [29]. Of the three independent B atoms, B3 adopts tetrahedral oxygen coordination and the other two B atoms are in triangular coordination. The B–O bond lengths in the tetrahedra range from 1.449(13) to 1.494(15) Å and the O–B–O angles from 102.7(9)° to 115.8(8)°; in the triangles, the respective ranges are 1.290(12)–1.440(10) Å and 117.1(8)°–124.0(9)°, as shown in Tables 3 and 4. These geometric parameters are comparable well with the data (1.476 and 1.370 Å for the tetrahedrally and trigonally coordinated boron atom, respectively), as obtained for borate minerals by Hawthorne et al. [30]. This compound features a three-dimensional framework constructed by $[B_3O_7]^{5-}$ groups, with hexagonal channels running parallel to [001] direction that are alternately occupied by Li^+ and Ba^{2+} cations, as shown in Fig. 2.

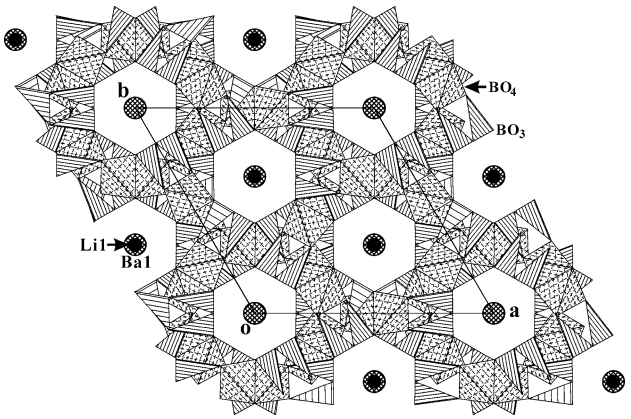

Fig. 2 Crystal structure of $LiBaB_9O_{15}$ projected along the [001] direction. Li atoms: *black circles*; Ba atoms: *circles with grid lines*; BO_4 groups: tetrahedra with crosses; BO_3 groups: *triangles with parallel lines*

The optimized structure of $LiBaB_9O_{15}$ single crystal has been used to calculate the electronic band structure, the atomic site-decomposed density of states, electron charge density and the chemical bonding features. The calculated electronic band structure shows that the valence band maxima (VBM) and the conduction band minima (CBM) are located at the center of the BZ. This confirms that the crystal is a direct wide band gap semiconductor. The value of the direct gap is 5.01 (5.11 eV) obtained using LDA (GGA), which is in good agreement with our experimental value measured from the UV–visible diffuse reflectance spectrum, showing a band gap of about 5.17 eV [15]. The electronic band structures for these different exchange correlation potentials are illustrated in Fig. 3(a) and 3(b). In the figures, it is noted that moving from LDA to GGA the CBM dramatically shifts toward higher energies, leading to a slightly bigger gap. The calculated effective mass ratio of heavy holes (m^*_{hh}/m_e), light holes (m^*_{lh}/m_e) in the valence band and electrons (m^*_e/m_e) in the conduction band minimum is 0.4670, 0.0973 and 0.0120, respectively.

The total and the atomic site-decomposed densities of states support the electronic band structure observation, as shown in Fig. 4(a)–4(f). The change in the energy gap can originate from a specific position of the conduction band minimum, which has strong cation-s states, whereas the other states in the conduction band are more admixtured with other atomic orbitals such as anion-*p* states. In the

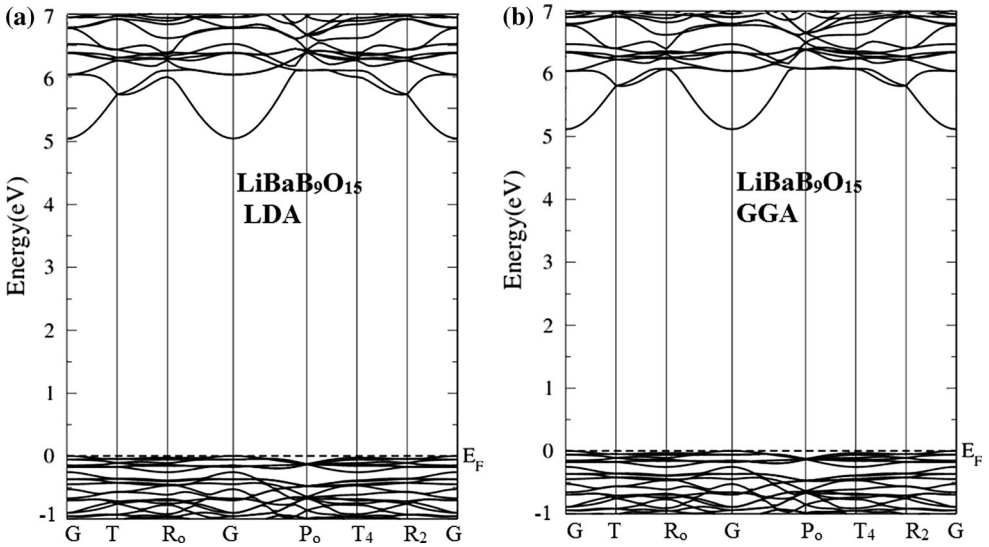

Fig. 3 Calculated band structure (**a**) LDA and (**b**) GGA

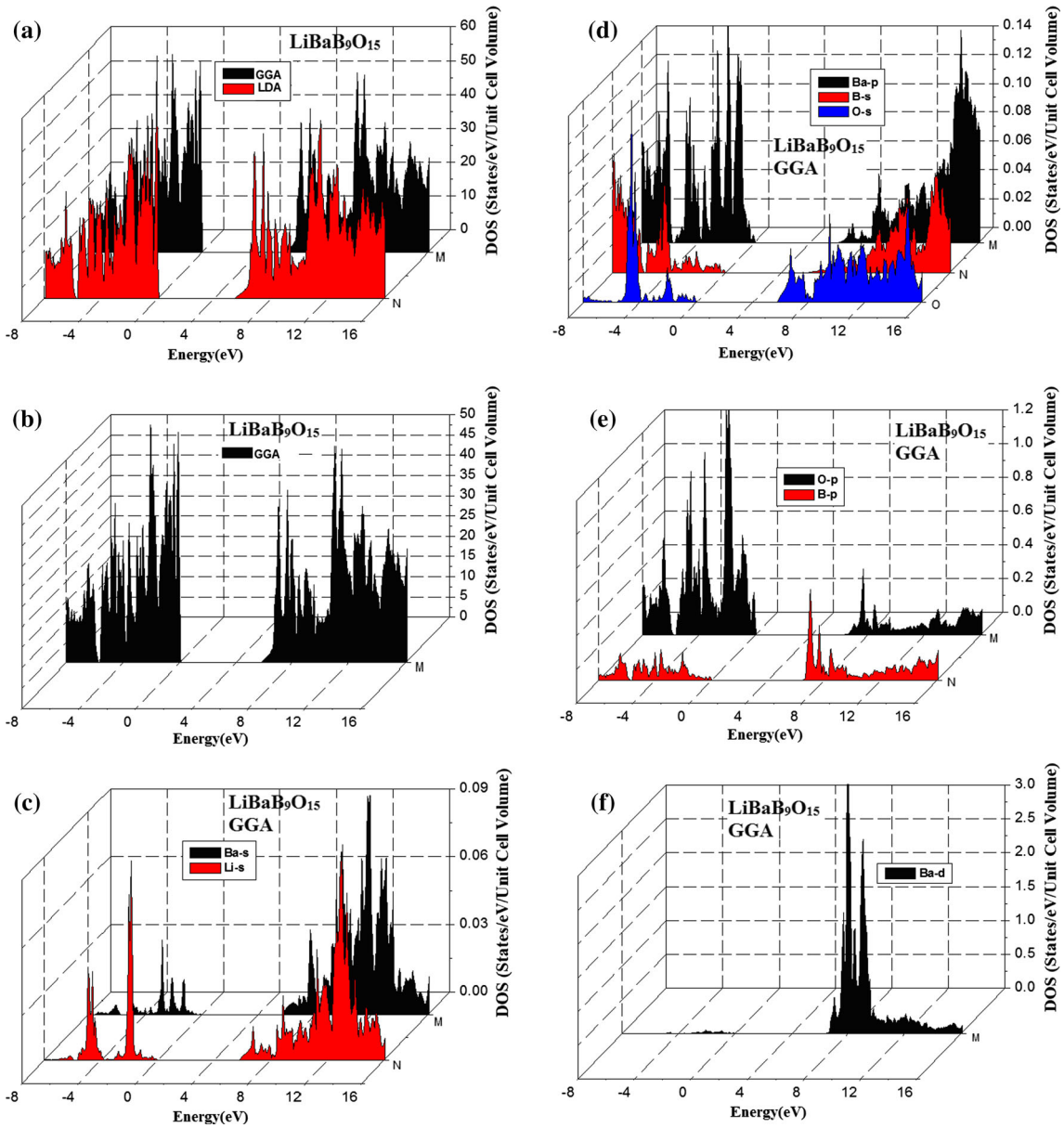

Fig. 4 Calculated total and partial densities of states (states/eV unit cell); (**a**) LDA and GGA; (**b**) GGA; (**c**) Ba-s and Li-s using GGA; (**d**) Ba-s/p and O-s using GGA; (**e**) O-p and B-p using GGA; (**f**) Ba-d using GGA

conduction bands, a shift of the CBM has a strong effect on decrease or increase in the energy gap.

From the angular momentum decomposition of the atom-projected density of states, one can see that there exists a strong hybridization between Ba-*p* and B-*s* states around −8.0 eV. The Ba-*p* state hybridizes with B-*s* and O-*s* states at around −4.2 eV. From −4.0 to −5.0 eV, there is also a strong hybridization between Ba-*p* and O-*s* sates. At conduction bands from 9.0 to 16.0 eV, Ba-s states hybridize with Li-*s* and O-*s*. Following the angular momentum decomposition of the atom-projected density of states, we have identified the angular momentum characters of various structures. The lowest energy group from −8.0 and −5.8 eV has mainly from O-p, Ba-p and B-s states with small contribution of B-p. The second group from −5.5 eV up to Fermi energy (E_f) originates mainly O-p, Ba-p and Li–s states with small admixture of B-p and Ba-s. The groups above E_f are mainly composed of Ba-s/p/d, Li-s and O-s.

To obtain a deeper insight into the electronic structure, we have displayed the electronic charge density contour in two crystallographic planes (1 0 0) and (1 1 0) in Fig. 5(a) and 5(b). The contour plot shows partial ionic and strong covalent bonding between O–O atoms. This can be

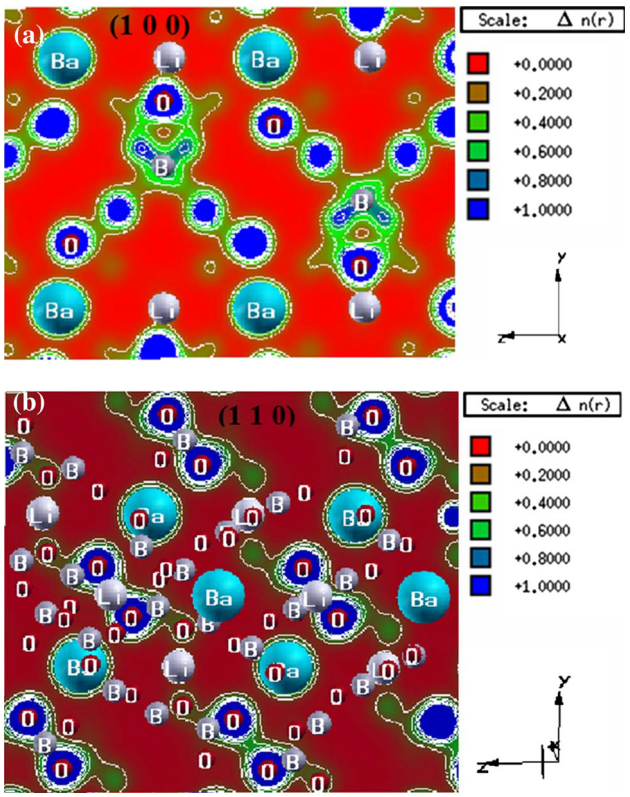

Fig. 5 Electronic charge density contours in (**a**) (1 0 0) plane and (**b**) (1 1 0) plane

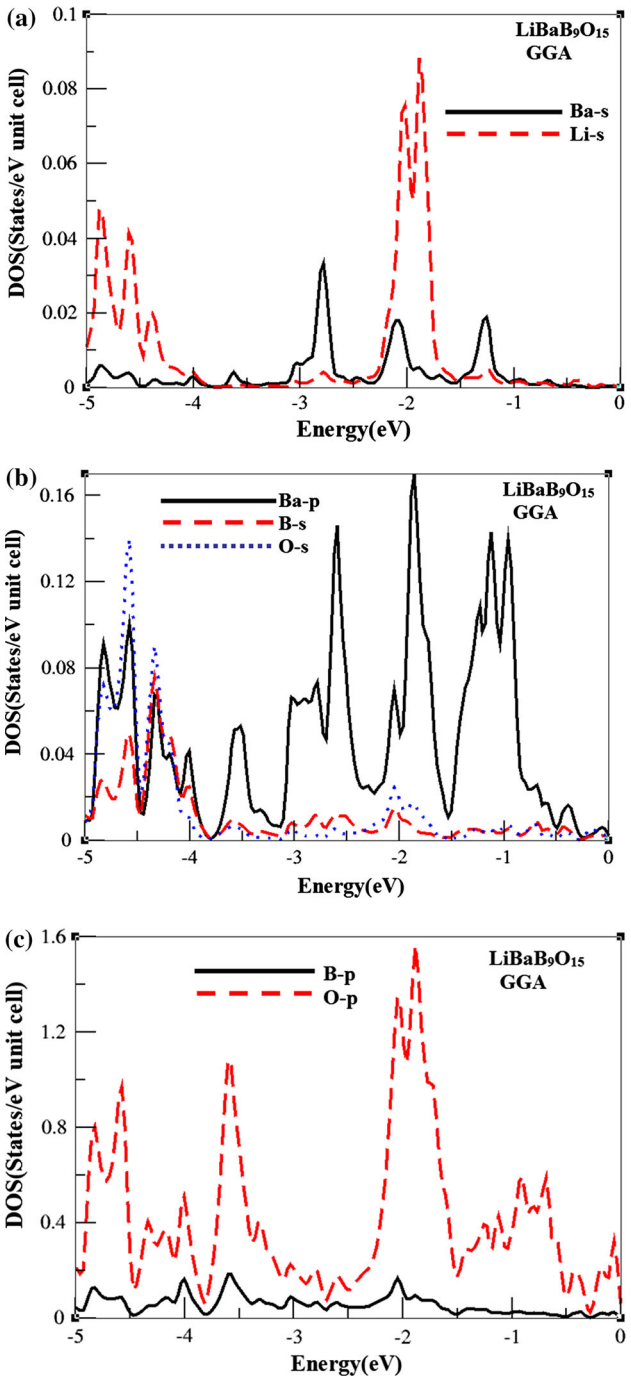

Fig. 6 Calculated partial densities of states (states/eV unit cell) below Fermi level; (**a**) Ba-s and Li–s using GGA; (**b**) Ba-s/p and O-s using GGA; (**c**) B-p and O-p using GGA

seen easily by the color charge density scale, where blue color (+1.0000) corresponds to the maximum charge accumulating site. The charge density along O–O bonds is pronounced. The Ba and Li atoms show ionic bonding. The two crystallographic planes (1 0 0) and (1 1 0), show considerable anisotropy. As we know that there exists a strong anisotropy in the crystal, when we change the plane the electronic charge density also changes. We have attempted to understand the reason of the anisotropy in the following. In the electronic charge density, there is covalent bonding between O atoms in (1 0 0) plane, while the O atoms show the ionic bonding in the (1 1 0) plane. Also, the charge density in the (1 0 0) plane around B atom is greater than that in (1 1 0) plane. Following these two contour plots in the (1 0 0) and (1 1 0) planes, one can see that this crystal possesses a strong anisotropy, which favors to enhance the optical susceptibilities and hence the second harmonic generation. As a consequence to this strong anisotropy, this crystal can be a promising material for NLO applications since it crystallizes in the non centrosymmetric space group.

The origin of chemical bonding can also be elucidated following the total and partial charge electronic density of states. This is obtained by comparing the total density of states with the angular momentum-projected density of states of Li, Ba, B and O atoms as shown in Fig. 6(a)–6(c). These results show that some electrons from Li, Ba, B and O atoms are transferred into valence bands (VBs) and contribute in covalence interactions between Li–Li, Ba–Ba, O–O and B–B atoms and the substantial covalent interactions between Li–O, B–O and Ba–O atoms. The covalent bond arises due to the degree of hybridization. It is clear

that there is an interaction of charges between Li–O, B–O and Ba–O atoms, due to the strong hybridization. Therefore, there is a strong covalent bonding between these atoms. Thus, the electronic density of states helps to analyze the nature of the bonds according to a classical chemical concept, which is very useful to classify compounds into different categories with respect to different chemical and physical properties. To support this statement, we have taken a more careful look at the bonding situation, since the existence of real hybridization between states of atoms should lead to covalent bond's origin between these atoms. We have calculated the bond lengths and angles. Good agreement has been found between the calculated bond lengths and angles with the measured ones, as shown in Tables 3 and 4.

5. Conclusions

The non-centrosymmetric $LiBaB_9O_{15}$ has been synthesized and characterized. The crystal contains $[B_3O_7]^{5-}$ groups composed of one BO_4 tetrahedra and two BO_3 triangles as the basic structural units that are condensed through the nonbridging O atoms to produce a 3D network, with the hexagonal channels hosting the Li^+ and Ba^{2+} cations. The existence of trigonally and tetrahedrally coordinated boron atoms has been further confirmed by IR spectrum. The atomic positions taken from our XRD data have been optimized by minimizing the forces acting on the atoms. Very good agreement has been found between the optimized atomic positions and measured ones. From the relaxed geometry, the electronic structure and the chemical bonding have been determined and various spectroscopic features have been simulated and compared with experimental data. The state-of-the-art, all-electron full-potential linearized augmented plane wave (FP-LAPW) method within the Ceperley–Alder LDA and the GGA has been used to solve the Kohn–Sham DFT equations. The calculated direct gap is about 5.01 (5.11 eV) using LDA (GGA), which shows good agreement with our experimental value (5.17 eV) obtained from the UV–visible diffuse reflectance spectrum. From the angular momentum decomposition of the atom-projected density of states, we have found that there exits a strong hybridization between orbitals. We have calculated the electronic charge density distribution and found that there exists considerable anisotropy between the two crystallographic planes (1 0 0) and (1 1 0). The calculated bond lengths and angles exhibit good agreements with experiment.

Acknowledgments The CENTEM Project, Reg. No. CZ.1.05/2.1.00/03.0088, co-funded by the ERDF as part of the Ministry of Education, Youth and Sports OP RDI program and, in the follow-up sustainability stage, supported through CENTEM PLUS (LO1402) by financial means from the Ministry of Education, Youth and Sports under the "National Sustainability Programme I" is acknowledged. Computational resources provided by MetaCentrum (LM2010005) and CERIT-SC (CZ.1.05/3.2.00/08.0144) infrastructures are also acknowledged. X. Chen thanks the National Natural Science Foundation of China (Grant No. 20871012) for support. SA would like to thank CSIR-NPL for financial support.

References

[1] B H Rudramadevi and S Buddhudu *Indian J. Phys.* **83** 313 (2009)
[2] V Aravindan and P Vickraman *Indian J. Phys.* **86** 341 (2012)
[3] B C Joshi, B Khulbey, D Upreti and C C Dhaundiyal *Indian J. Phys.* **84** 405 (2010)
[4] K N Shinde, I M Nagpure, S J Dhoble, S V Godbole and M K Bhide *Indian J. Phys.* **83** 503 (2009)
[5] P Becker *Adv. Mater.* **10** 979 (1998)
[6] Z-B Lin, Z-S Hu and G-F Wang *Chin. J. Struct. Chem.* **20** 256 (2001)
[7] S-K Pan, G-F Wsng and Z-X Huang *Chin. J. Struct. Chem.* **21** 382 (2002)
[8] C T Chen, B Wu, A Jiang and G You *Sci. China B* **18** 235 (1985)
[9] C T Chen et al. *J. Opt. Soc. Am. B* **6** 616 (1989)
[10] C T Chen, Y Wang, B Wu, K Wu, W Zeng and L Yu *Nature* **373** 322 (1995)
[11] W-D Cheng, H Zhang, Q-S Lin, F-K Zheng and J-T Chen *Chem. Mater.* **13** 1841 (2001)
[12] Q Huang, S Lu, G Dai and J Liang *Acta Crystallogr. C* **48** 1576 (1992)
[13] N Penin, L Seguin, M Touboul and G Nowogrocki *Inter. J. Inorg. Mater.* **3** 1015 (2001)
[14] D Yu Pushcharovsky, E R Gobetchia, M Pasero, S Merlino and O V Dimitrova *J. Alloys Compd.* **339** 70 (2002)
[15] A H Reshak et al. *J. Phys. Chem. B* **117** 14141 (2013)
[16] A M El-Naggar et al. *J. Cryst. Growth* **334** 122 (2011)
[17] I V Kityk et al. *J. Phys. Chem. B* **110** 9090 (2006)
[18] I V Kityk, A Majchrowski, J Zmija, Z Mierczyk, K Nouneh *Cryst. Growth Des.* **6** 2779 (2006)
[19] A Majchrowski, A Mandowska, I V Kityk, M G Brik and I Sildos *Curr. Opin. Solid State Mater. Sci.* **12** 32 (2009)
[20] Rigaku/AFC Diffractometer Control Software, Rigaku Corporation (1994)
[21] G M Sheldrick *Acta Crystallogr. A* **64** 112 (2008)
[22] G M Sheldrick, SHELX-97: program for structure refinement. (Germany: University of Goettingen) (1997)
[23] P Blaha, K Schwarz, G K H Madsen, D Kvasnicka and J Luitz *WIEN2 K, "an Augmented Plane Wave + Local orbitals program for calculating crystal properties"*, (Wien, Austria: Karlheinz Schwarz, Techn. Universitat) (2001) ISBN 3-9501031-1-2
[24] P Hohenberg and W Kohn *Phys. Rev. B* **136** 864 (1964)
[25] D M Ceperley and B I Ader *Phys. Rev. Lett.* **45** 566 (1980)
[26] J P Perdew and A Zunger *Phys. Rev. B* **8** 4822 (1973)
[27] J P Perdew, S Burke and M Ernzerhof *Phys. Rev. Lett.* **77** 3865 (1996)
[28] I D Brown and D. Altermatt *Acta Crystallogr. B* **41** 244 (1985)
[29] R D Shannon *Acta Crystallogr. A* **32** 751 (1976)
[30] F C Hawthorne, P C Burns and J D Grice *Rev. Miner.* **33** 41 (1996)